Quasi-elastic scattering of ^{10,11}C and ^{10}B from a ^{nat}Pb target

Y. Y. Yang,[1,*] J. S. Wang,[1,†] Q. Wang,[1] D. Y. Pang,[2,3] J. B. Ma,[1] M. R. Huang,[1] P. Ma,[1] S. L. Jin,[1,4] J. L. Han,[1] Z. Bai,[1,4] L. Jin,[1,4] J. B. Chen,[1,4] Q. Hu,[1,4] R. Wada,[1] S. Mukherjee,[5] Z. Y. Sun,[1] R. F. Chen,[1] X. Y. Zhang,[1] Z. G. Hu,[1] X. H. Yuan,[1] S. W. Xu,[1] S. Z. Chen,[1,4] X. G. Lei,[1] L. X. Liu,[1,4] W. H. Ma,[1,4] S. T. Wang,[1] D. Yan,[1,4] X. H. Zhang,[1] M. H. Zhao,[1,4] Y. Zhou,[1,4] Y. J. Zhou,[1,4] Z. Y. Guo,[1] Y. H. Zhang,[1] H. S. Xu,[1] and G. Q. Xiao[1]

[1]*Institute of Modern Physics, Chinese Academy of Sciences, Lanzhou 730000, China*

[2]*School of Physics and Nuclear Energy Engineering, Beihang University, Beijing 100191, China*

[3]*International Research Center for Nuclei and Particles in the Cosmos, Beihang University, Beijing 100191, China*

[4]*University of Chinese Academy of Sciences, Beijing 100049, China*

[5]*Physics Department, Faculty of Science, M.S. University of Baroda, Vadodara 390002, India*

(Received 9 June 2014; published 16 July 2014)

Angular distributions of the differential cross sections for the quasi-elastic scattering from a ^{nat}Pb target by ^{10}C at 226 and 256 MeV, by ^{11}C at 222 MeV and 226 MeV, and by ^{10}B at 173 MeV were measured at the Heavy Ion Research Facility in Lanzhou, Radioactive Ion Beam Line in Lanzhou (HIRFL-RIBLL). Contributions from the inelastic scattering channels to these data are found to be negligibly small with coupled-channel calculations within the angular range covered by this experiment. These data can be well reproduced by optical model calculations with systematic nucleus-nucleus potentials. The reduced total reaction cross sections were compared with other existing data.

DOI: 10.1103/PhysRevC.90.014606 PACS number(s): 24.10.Ht, 25.60.Bx, 25.70.Bc

I. INTRODUCTION

Elastic scattering is one of the most important channels to be measured for studies of nuclear structure via nuclear reactions since it can be used to constrain the optical model potentials (OMPs) that are necessary for generating the distorted waves of the entrance and exit channels [1]. Besides such practical purposes, studies of OMPs themselves are interesting subjects for nuclear physics [2–7]. Due to these reasons, measurements of elastic scattering are important for nuclear studies. Over many years, a lot of elastic scattering measurements have performed, especially for light projectiles, such as proton, neutron, deuteron, triton, helion, and α particles. Out of which many systematic optical potentials have been derived [8–14]. However, the experimental data for heavier particles, especially for those light-heavy ions with atomic mass numbers around 10, are still not sufficient for systematic studies. Recently a project which aimed to make systematic measurements of elastic scattering of light-heavy ions, especially those near the proton-drip line, was established at the Heavy Ion Research Facility in Lanzhou [15,16], Radioactive Ion Beam Line in Lanzhou [17,18] (HIRFL-RIBLL). Experimental data of ^{7}Be and ^{8}B scattering from a natural lead target at around 20 MeV/nucleon have been reported [19,20].

Recently, there has been increasing interest in the study of the elastic scattering induced by light radioactive ion beams. Some new interesting phenomena are discovered. Strong Coulomb rainbow suppressions are found for neutron halo nuclei such as ^{11}Be [21], ^{11}Li [22], and ^{6}He [23–26] elastic scattering from heavy targets at energy near Coulomb barrier. However this phenomenon is not observed in ^{8}B + ^{nat}Pb elastic scattering at an energy about three times the Coulomb barrier [20]. The same phenomena have also been observed in other proton-rich nuclei, such as ^{17}F [27]. This may indicate that there are some systematic differences in the diffraction patterns of the angular distributions of elastic scattering cross sections induced by proton- and neutron-rich nuclei. Numerous experiments have been made for neutron-rich nuclei, however, there are few experimental data for proton-rich unstable nuclei. In this paper we report our results for ^{10}Be, ^{10}C, and ^{11}C elastic scattering from ^{nat}Pb at the same energy region. Due to the limitation of experimental techniques, these data are quasi-elastic in nature. However, as we demonstrate in this paper, the contributions from inelastic scattering channels are negligibly small within the angular range covered in our measurements. Because of this, for simplicity, we will sometimes use the term "elastic scattering" for our data.

This paper is organized as follows. the experimental details are given in Sec. II. Results of optical model analysis by using both systematic folding potentials and phenomenological Woods-Saxon potentials are reported in Sec. III. Our conclusions are given in Sec. IV.

II. EXPERIMENT

The measurements were carried out using the ^{10}C, ^{11}C, and ^{10}B beams provided by RIBLL. The secondary beams of radioactive isotopes were produced by the fragmentation of the (54 MeV/nucleon) ^{12}C primary beam, separated by their magnetic rigidity using HIRFL, on a 2652 μm Be target. The energies of the secondary beams, at the physical target, were 226 and 256 MeV for ^{10}C, 226 and 226 MeV for ^{11}C, and 173 MeV for ^{10}B. The energy resolutions (σ) of these secondary beams were 0.7%. The ^{10}B (173 MeV) and ^{11}C (226 MeV) beams had the same magnetic rigidity of

*yangyanyun@impcas.ac.cn
†jswang@impcas.ac.cn

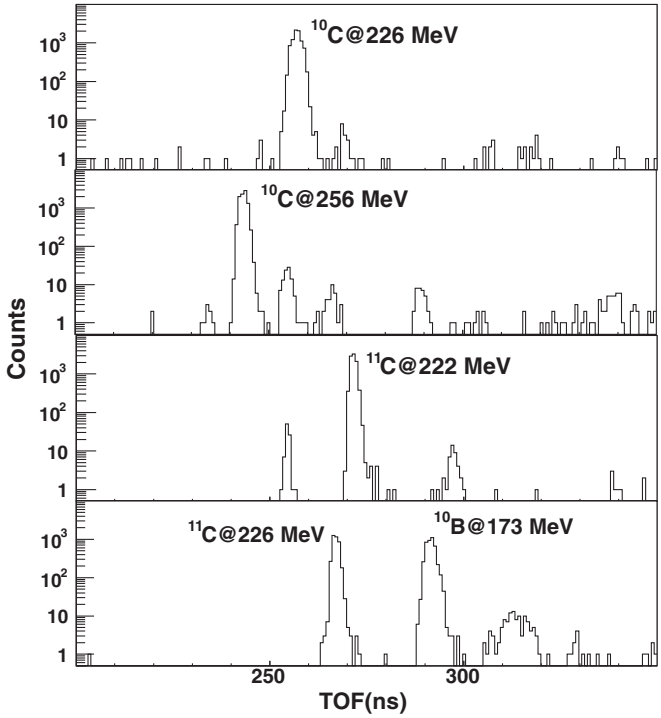

FIG. 1. Time-of-flight (TOF) spectrum of the secondary beams in this experiment. Particles and their incident energies are indicated in these figures.

RIBLL. Self-supporting foils of ^{nat}Pb with a thickness of 4.2 mg/cm^2 was used. The target had the following isotopic composition: ^{208}Pb 52.3%, ^{207}Pb 22.6%, ^{206}Pb 23.6%, and ^{204}Pb 1.48%. The typical primary beam current was 200 enA, giving typical secondary beam rates for ^{10}C, ^{11}C, and ^{10}B of 3×10^4, 4×10^4, and 2×10^4 particles per second, respectively. The spot size of beam on target was about 30 mm in diameter. Time of flight (TOF) with a flight path of 17 m was used for the beam particle identification. The typical TOF spectra for the secondary beams are shown in Fig. 1. The secondary beams can be clearly identified in the offline data analysis by applying cuts the TOF spectra.

A schematic lay-out of the experiment setup is shown in Fig. 2. Two position-sensitive parallel-plate avalanche counters (PPACs) with a position resolution of 1 mm were used to reconstruct the position and incident angle of the incoming beam at the target event by event. Each PPAC has 80 gold-plated tungsten wires, 20 μm in diameter, in both X and Y directions and therefore the sensitive area is 80×80 mm^2. The PPACs distances from the target were 500 mm and 100 mm, respectively. The beam spot and beam divergence on the target,

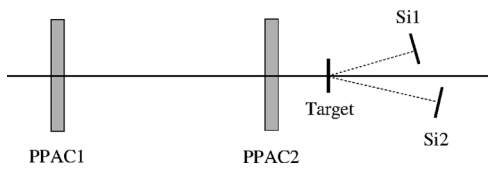

FIG. 2. Schematic lay-out of the experimental setups.

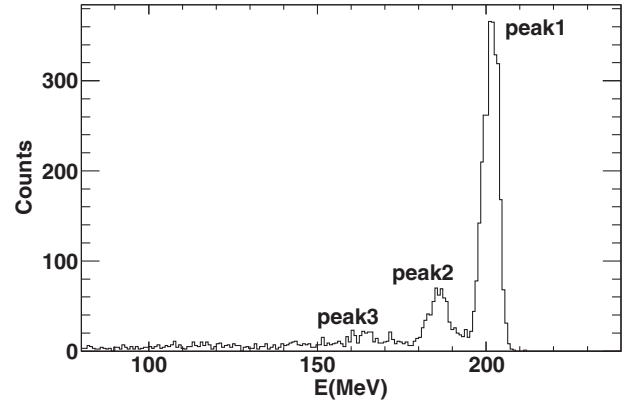

FIG. 3. One-dimensional energy spectrum for ^{10}C at 226 MeV obtained with a SSD. The three peaks were generated from the elastic scattering on the ^{nat}Pb target (peak1), from scattered on a tungsten wire of PPACs (peak2), and from scattered on double-sequential hits on the tungsten wires (peak3), respectively.

measured with these PPACs, are 30 mm in diameter and the 35 mrad, respectively.

The scattered particles were detected by two sets of ΔE-E detector telescopes (denoted by Si2 and Si1 in Fig. 2). The distances from the ^{nat}Pb target to the center of the telescopes were 247 and 201 mm, respectively. Each telescope consists of one double-sided silicon strip detector (DSSD) and a single silicon detector (SSD). The 150 μm thick DSSD has 48 strips, which are 48 mm long and 1 mm wide on both the front and the back sides, and has 48×48 mm^2 in area. The angle range covered corresponded to $\theta_{lab} = 7^\circ$–30°. However, the statistics were very low at larger angles. The SSD is 1500 μm thick and was 50×50 mm^2 in area. A typical energy spectrum for ^{10}C obtained with a SSD is presented in Fig. 3. The three peaks were observed and they originated from the elastic scattering on the ^{nat}Pb target (peak1), from scattered on a tungsten wire of PPACs (peak2), and from scattered on double-sequential hits on the tungsten wires (peak3), respectively. The elastic scattering events were separated clearly.

The actual position and direction of the beam on the target are provided by connecting the two hit points on the PPACs and extending to the target plane. The scattering angle is obtained from the position and direction of the beam and the hit point on the telescopes. Because of the broad and nonuniform beam profiles, the solid angles cannot be calculated directly. Therefore, a Monte Carlo simulation is used to evaluate the absolute differential cross sections. The elastic scattering differential cross section $d\sigma(\theta)$ as the ratio to the Rutherford cross section $d\sigma(\theta)_{\rm Ruth}$ is obtained by

$$\frac{d\sigma(\theta)}{d\sigma_{\rm Ruth}(\theta)} = C\frac{N(\theta)_{\rm exp}}{N(\theta)_{\rm Ruth}}, \quad (1)$$

where C is a normalization constant, $N(\theta)_{\rm exp}$ and $N(\theta)_{\rm Ruth}$ are the yields at a given angle from the experiment and the simulation, respectively. The constant C is a global normalization factor of the angular distributions of the elastic scattering cross sections, and it was determined by imposing that at

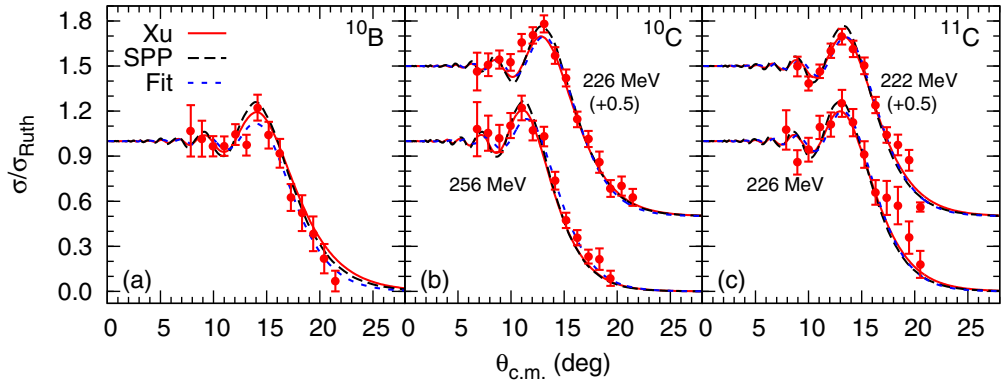

FIG. 4. (Color online) Comparisons between experimental data and optical model calculations with systematic nucleus-nucleus potentials for (a) ^{10}B, (b) ^{10}C, and (c) ^{11}C from the lead target. The systematic potentials are that of Xu in Ref. [28] (solid curves) and SPP in Ref. [7] (dashed curves). Results of phenomenological potentials by fitting the experimental data are also shown in dotted curves.

small scattering angles, the ratio of elastic and Rutherford cross sections becomes independent of θ and equal to unity. In order to properly reconstruct the angular distributions, small corrections for detectors misalignments had to be performed. The elastic scattering yield at a given angle was correct for the detectors misalignments using a method described in Ref. [19]. This method provides an effective position of the detectors by imposing the pure Rutherford scattering at very forward angles. In the experiment, the elastic scattering angular distributions were taken in two separate ΔE-E telescopes, and then pieced together with the overlapping points between the two sets of data. In Fig. 4 the angular distributions of the elastic scattering resulting from our data analysis are presented. The error bars shown are the statistical errors, which are the dominant source of the error. The total energy resolution (energy resolution of the SSDs and energy dispersion of secondary beam) was insufficient to separate elastic from inelastic scattering events. However, as we see in the following section, the inelastic channel contributes little to the angular distributions of the elastic scattering.

III. OPTICAL MODEL ANALYSIS

Recently, a systematic nucleus-nucleus potential has been proposed, which gives a reasonable account for elastic scatterings and total reaction cross sections for projectiles with atomic mass numbers up to $A \lesssim 40$, including both stable and unstable nuclei, for incident energies above the Coulomb barrier [28]. Optical model calculations with this systematic nucleus-nucleus potential and their comparison with experimental data are shown by solid lines in Fig. 4. The total reaction cross sections are 3206 mb, 3342 mb, 3414 mb, 3334 mb, and 3348 mb for ^{10}B, ^{10}C at 226 MeV, ^{10}C at 256 MeV, ^{11}C at 222 MeV, and ^{11}C at 226 MeV, respectively. For comparisons, results of calculations with the systematic São Paulo potential (SPP) [7] are also presented by dashed lines. Clearly, both of the systematic potentials give a good account for the angular distributions and elastic scattering cross sections. The corresponding total reaction cross sections with the SPP are 3162 mb, 3178 mb, 3269 mb, 3250 mb, and 3266 mb, respectively, which are, on average, 3% smaller than that of the systematics in Ref. [28].

Since none of the excited states of the scattered particles and the target nucleus were discriminated from their ground states, the experimental data are of quasi-elastic nature. The contributions from the excited states of the lead target have been found to be negligible in the angular range covered by this experiment, as those reported in Ref. [20] in the study of ^{8}B elastic scattering. Unlike ^{8}B, which does not have bound excited states so that the detected ^{8}B particles in the exit channel are all in their ground states, the ^{10}B, ^{10}C, and ^{11}C particles have bound excited states. Particles in these excited states are all counted in the quasi-elastic scattering data reported in this paper. In order to examine the contributions from the inelastic channels, coupled-channel calculations were preformed with the computer code FRESCO [31]. The rotational model was used in all the following three cases, which takes into account the first few bound excited states permitted by the E_2 transition from their ground states. The excited states included in these calculations are 1^+ (0.717 MeV), 1^+ (2.154 MeV), 3^+ (4.774 MeV) for ^{10}B [29], 2^+ (3.354 MeV) for ^{10}C [30], and $\frac{5}{2}^-$ (4.33 MeV) and $\frac{7}{2}^-$ (6.48 MeV) for ^{11}C [30]. These calculations are made with deformation length $\delta_2 = 1.8$ fm for ^{10}B, $B(E2) = 61.5\, e^2$ fm^4 for ^{10}C, $B(E2) = 10.88\, e^2$ fm^4 for the $\frac{5}{2}^-$ state of ^{11}C, and $B(E2) = 15.48\, e^2$ fm^4 for the $\frac{7}{2}^-$ state in ^{11}C [29,30]. The resulting inelastic scattering cross sections, as ratio to the Rutherford cross sections, are depicted in Fig. 5 together with their corresponding elastic scattering cross sections. Clearly we can conclude that the contributions from the inelastic scattering channels are negligible in the quasi-elastic scattering data within the angular range covered by our measurement. A systematic nucleus-nucleus potential in Ref. [28] was used in these calculations.

Although both of the systematic potentials in Refs. [28] and [7] reproduce experimental data fairly well, these forms of folding potentials are not generally available by the nuclear physics community, especially by experimental groups. In Table I we present the parametrized potentials for these five cases, which are obtained by fitting experimental data with the

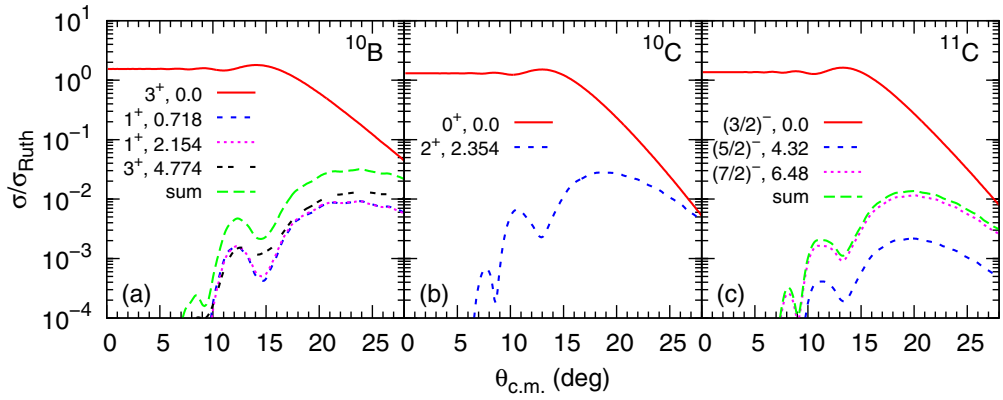

FIG. 5. (Color online) Angular distributions of elastic and inelastic scattering cross sections for (a) ^{10}B at 173 MeV, (b) ^{10}C at 226 MeV, and (c) ^{11}C at 222 MeV from the lead target. Spin-parity and excitation energies of the states included in the coupled-channel calculations are indicated in the figures. Summations of these inelastic scattering cross sections are shown as dashed curves. See text for the details.

following form factors:

$$U(r) = V(r) + iW(r) + V_C(r), \tag{2}$$

where the real nuclear potential has the usual volume Woods-Saxon form

$$V(r) = -\frac{V}{1 + e^{(r-R_v)/a_v}}, \tag{3}$$

the imaginary part has both volume and surface terms

$$W(r) = -\frac{W_v}{1 + e^{(r-R_{wv})/a_{wv}}} - \frac{4W_s e^{(r-R_{ws})/a_w s}}{\left[1 + e^{(r-R_{ws})/a_{ws}}\right]^2}, \tag{4}$$

in which, the radii of these potentials are $R_{v,wv,ws} = r_{v,wv,ws}(A_P^{1/3} + A_T^{1/3})$, where A_P and A_T are the mass numbers of the projectile and the target nuclei ($A_T = 208$). The Coulomb potential V_C is taken to be that of a uniformly charged sphere of radius $R_C = r_C(A_P^{1/3} + A_T^{1/3})$. The fittings were made with the usual minimum χ^2 criteria. Experimental error bars were used in evaluating the χ^2 values. Only parameters a_v, a_{wv}, and a_{ws} in Table I are varied during the fittings with the experimental data. All other parameters are kept fixed as the result of fitting the systematic potentials of Ref. [28] using form factors in Eqs. (3) and (4). Note that these parameters are not unique due to the well-known ambiguities in optical potentials with experimental data measured within a limited angular range. The total reaction cross sections corresponding to these parameters are also given in Table I.

TABLE I. Optical model parameters obtained by minimum χ^2 fitting of experimental data. Incident energies and potential depthes are given in MeV, geometrical parameters are given in fm, and total reaction cross sections are given in b. The χ^2 values are χ^2-per-data-point.

Projectile	^{10}B	^{10}C	^{10}C	^{11}C	^{11}C
E_{lab}	173	226	256	222	226
V	251.3	261.6	263.9	282.3	282.6
r_v	0.851	0.848	0.847	0.841	0.841
a_v	0.940	0.954	0.854	0.937	0.937
W_v	31.7	41.0	47.1	40.1	40.8
r_{wv}	0.830	0.824	0.819	0.819	0.818
a_{wv}	1.527	1.017	1.015	0.989	0.984
W_s	47.9	48.5	46.8	52.5	52.4
r_{ws}	0.830	0.824	0.819	0.819	0.818
a_{ws}	0.844	1.010	0.989	0.998	0.995
σ_R	3.691	3.352	3.360	3.356	3.354
χ^2	0.53	1.53	0.55	1.79	1.21

In order to compare the total reaction cross sections with other existing data [20,32–37], a reduction method [38] was used. The total reaction cross sections and the incident energies are divided by $(A_P^{1/3} + A_T^{1/3})^2$ and $Z_P Z_T/(A_P^{1/3} + A_T^{1/3})$, respectively, where Z_P (A_P) and Z_T (A_T) are the charges (mass) of the projectiles and targets, respectively. With this method, the geometrical and charge effects were minimized without disturbing the physical processes or specific features of the projectile nuclear matter density. The results are presented in Fig. 6. The reduced cross sections of the halo projectile system (^{8}B) are strikingly different from those of other systems at the energies around/below the Coulomb barrier. However, there are no distinct differences among halo, weakly bound, and stable projectiles at above the barrier energies. This

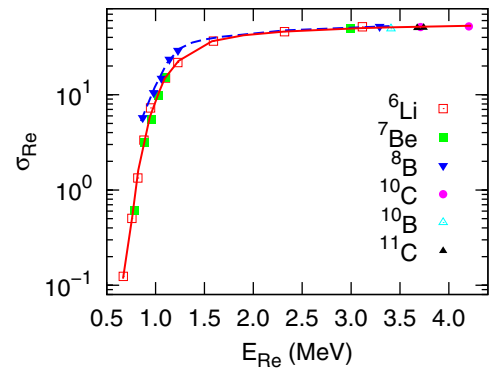

FIG. 6. (Color online) Reduced total reaction cross sections, σ_{Re}, from the present work and other measurements [20,32–37] with respect to the reduced incident energy, E_{Re}. The curves are to guide the eye.

may indicate that the effects of the weak binding energy are switching on additional reaction channels that would enhance the total reaction cross sections at the energies around the Coulomb barriers. On the other hand we can conclude that, at higher incident energies, the influence of the additional channels couplings on the total reaction cross sections is small.

IV. SUMMARY

In this paper, we report the angular distributions of the quasi-elastic scattering cross sections of ^{10}C at 226 and 256 MeV, ^{11}C at 222 and 226 MeV, and ^{10}B at 173 MeV from a ^{nat}Pb target. Contributions from the inelastic scattering channels in the experimental data were found to be negligible with the coupled channel calculations. Optical model calculations using the systematic nucleus-nucleus potentials of both Ref. [28] and SPP were performed. The results of our calculations are in good agreement with the experimental results. We have also compared the reduced total reaction cross sections with some other existing data. It is found that the reduced reaction cross sections for exotic, weakly bound nuclei, and tightly bound nuclei follow the same trend at energies around 3 times of Coulomb barriers.

ACKNOWLEDGMENTS

We would like to acknowledge the staff of HIRFL for the operation of the cyclotron and friendly collaboration. This work was financially supported by the National Basic Research Program of China (973 program, 2014CB845405) and the National Natural Science Foundation of China (Nos. 11275018, 11021504, 11035001, 11275018, 11205209, and 11205221).

[1] G. R. Satchler, *Direct Nuclear Reactions* (Oxford University Press, New York, 1983).
[2] C. Mahaux, H. Ngô, and G. R. Satchler, Nucl. Phys. A **449**, 354 (1986).
[3] D. F. Jackson and R. C. Johnson, Phys. Lett. B **49**, 249 (1974).
[4] G. R. Satchler and W. G. Love, Phys. Rep. **55**, 183 (1979).
[5] M. E. Brandan and G. R. Satchler, Phys. Rep. **285**, 143 (1997).
[6] L. C. Chamon, D. Pereira, M. S. Hussein, M. A. Cândido Ribeiro, and D. Galetti, Phys. Rev. Lett. **79**, 5218 (1997).
[7] L. C. Chamon *et al.*, Phys. Rev. C **66**, 014610 (2002).
[8] F. D. Becchetti Jr. and G. W. Greenlees, Phys. Rev. **182**, 1190 (1969).
[9] R. L. Varner *et al.*, Phys. Rep. **201**, 57 (1991).
[10] A. J. Koning and J. P. Delaroche, Nucl. Phys. A **713**, 231 (2003).
[11] W. W. Daehnick, J. D. Childs, and Z. Vrcelj, Phys. Rev. C **21**, 2253 (1980).
[12] D. Y. Pang, P. Roussel-Chomaz, H. Savajols, R. L. Varner, and R. Wolski, Phys. Rev. C **79**, 024615 (2009).
[13] Xiaohua Li, Chuntian Liang, and Chonghai Cai, Nucl. Phys. A **789**, 103 (2007).
[14] D. Y. Pang, Y. L. Ye, and F. R. Xu, Phys. Rev. C **83**, 064619 (2011).
[15] J. W. Xia *et al.*, Nucl. Instrum. Methods Phys. Res. A **488**, 11 (2002).
[16] W. L. Zhan *et al.*, Nucl. Phys. A **805**, 533c (2008).
[17] Z. Sun *et al.*, Chin. Phys. Lett. **15**, 790 (1998).
[18] Z. Sun *et al.*, Nucl. Instrum. Methods Phys. Res. A **503**, 496 (2003).
[19] Y. Y. Yang *et al.*, Nucl. Instrum. Methods Phys. Res. A **701**, 1 (2013).
[20] Y. Y. Yang, J. S. Wang, Q. Wang, D. Y. Pang *et al.*, Phys. Rev. C **87**, 044613 (2013).
[21] A. Di Pietro *et al.*, Phys. Rev. Lett. **105**, 022701 (2010).
[22] M. Cubero *et al.*, Phys. Rev. Lett. **109**, 262701 (2012).
[23] E. F. Aguilera *et al.*, Phys. Rev. C **63**, 061603(R) (2001).
[24] O. R. Kakuee *et al.*, Nucl. Phys. A **691**, 599 (2001).
[25] A. Di Pietro *et al.*, Phys. Rev. C **69**, 044613 (2004).
[26] L. Acosta *et al.*, Phys. Rev. C **84**, 044604 (2011).
[27] J. F. Liang, J. R. Beene, H. Esbensen, A. Galindo-Uribarri, J. Gomez del Campo, C. J. Gross, M. L. Halbert, P. E. Mueller, D. Shapira, D. W. Stracener, I. J. Thompson, and R. L. Varner, Phys. Rev. C **65**, 051603(R) (2002).
[28] Y. P. Xu and D. Y. Pang, Phys. Rev. C **87**, 044605 (2013).
[29] A. T. Rudchik, V. O. Romanyshyn, E. I. Koshchy, A. Budzanowski *et al.*, Eur. Phys. J. A **33**, 317 (2007).
[30] C. Jouanne, V. Lapoux, F. Auger, N. Alamanos, A. Gillibert *et al.*, Phys. Rev. C **72**, 014308 (2005).
[31] I. J. Thompson, Comp. Phys. Rep. **7**, 167 (1988).
[32] E. F. Aguilera *et al.*, Phys. Rev. C **79**, 021601(R) (2009).
[33] D. P. Stanley, F. Petrovich, and P. Schwandt, Phys. Rev. C **22**, 1357 (1980).
[34] Zhang Chun-Lei *et al.*, Chin. Phys. Rev. **23**, 1146 (2006).
[35] N. Keeley, J. M. Cook, K. W. Kemper, B. T. Roeder, W. D. Weintraub, F. Marechal, and K. Rusek, Phys. Rev. C **68**, 054601 (2003).
[36] L. T. Chua *et al.*, Nucl. Phys. A **273**, 243 (1976).
[37] R. Huffman, A. Galonsky, R. Markham, and C. Williamson, Phys. Rev. C **22**, 1522 (1980).
[38] P. R. S. Gomes, J. Lubian, I. Padron, and R. M. Anjos, Phys. Rev. C **71**, 017601 (2005).